RSC Advances

PAPER

View Article Online
View Journal | View Issue

Cite this: *RSC Adv.*, 2020, **10**, 19466

The fabrication of mechanically durable and stretchable superhydrophobic PDMS/SiO_2 composite film†

Chao-Hua Xue, *[ab] Qian-Qian Tian,[a] Shun-Tian Jia,[a] Ling-Ling Zhao,[a] Ya-Ru Ding,[a] Hui-Gui Li[a] and Qiu-Feng An[c]

Received 3rd March 2020
Accepted 6th May 2020

DOI: 10.1039/d0ra02029j

rsc.li/rsc-advances

Stretchable superhydrophobic film was fabricated by casting silicone rubber polydimethylsiloxane (PDMS) on a SiO_2 nanoparticle-decorated template and subsequent stripping. PDMS endowed the resulting surface with excellent flexibility and stretchability. The use of nanoparticles contributed to the sustained roughening of the surface, even under large strain, offering mechanically durable superhydrophobicity. The resulting composite film could maintain its superhydrophobicity (water contact angle ≈ 161° and sliding angle close to 0°) under a large stretching strain of up to 100% and could withstand 500 stretching–releasing cycles without losing its superhydrophobic properties. Furthermore, the obtained film was resistant to long term exposure to different pH solutions and ultraviolet light irradiation, as well as to manual destruction, sandpaper abrasion, and weight pressing.

1 Introduction

Superhydrophobic surfaces with a water contact angle (CA) greater than 150° and a sliding angle (SA) smaller than 10° have attracted considerable attention in the past few decades,[1–5] with the SA being analyzed by the Wolfram approach.[6] Inspiration from natural non-wetting structures, particularly the leaves of lotus plants[7,8], has led to numerous applications in self-cleaning,[9–11] dragging reduction,[12,13] oil–water separation[14–16] and corrosion resistance.[17–19] Representative examples of non-wetting prototypes in nature not only include the leaves of lotus plants, but also pond skater legs[20,21] and butterfly wings.[22] Research shows that such surfaces largely depend on hierarchical roughness with micro- and nanoscale structures and low-surface-energy components.[23–26] Over the last few decades, a large number of studies relating to durable superhydrophobic materials have been reported.[27–32] Many methods have been dedicated to the production of stable and durable superhydrophobic material, which can be divided into two categories. One method involves integrating a self-healing ability into superhydrophobic materials, including relocating of hydrophobic components or recombining topographic structures,[33–40] resulting in the restoration of their superhydrophobicity. Due to the limited number of hydrophobic components, the repairing cycles in this approach are limited. Furthermore, the self-healing process requires certain specific conditions in terms of light and temperature, and time (from tens of minutes to hours).[37,38,40] Hence, the application of this approach is limited. The second method is to use expensive low-surface-free energy compounds. Fluorine-containing low surface-energy materials are used to improve the stability of superhydrophobic materials.[41,42] However, fluorinated compounds have been identified as a source of toxic pollutants, which are harmful to the environment and increase the chances of many intractable diseases (*e.g.*, cancer). Therefore, it is necessary to develop a new method to fabricate durable superhydrophobic materials.

Most such reports are on rigid substrates or flexible substrates with low deformation ability. The micro-nanostructures on the surface are mostly fragile and easily lose their anti-wetting characteristics under large mechanical deformation (>50%).[43,44] Hence, maintaining superhydrophobicity under large mechanical deformation still poses considerable challenges. Hard substrates have been replaced by highly stretchable substrates to fabricate durable superhydrophobic materials.[45–47] Furthermore, due to rapid developments in the stretchable electronic industry, superhydrophobic surfaces based on flexible substrates have become candidates to meet the demands of modern industry. Mates *et al.* achieved a conductive and stretchable superhydrophobic material by spraying carbon nanotubes-Parafil-M (a commercial paraffin wax–polyolefin thermoplastic blend) composite on natural rubber.[47] Cho *et al.* prepared a gas-breathable superhydrophobic membrane with stretchability *via* three steps, including electrospinning, construction of micro-

[a]College of Bioresources Chemical and Materials Engineering, Shaanxi University of Science and Technology, Xi'an 710021, China. E-mail: xuechaohua@126.com
[b]National Demonstration Center for Experimental Light Chemistry Engineering Education, Shaanxi University of Science and Technology, Xi'an 710021, China
[c]College of Chemistry and Chemical Engineering, Shaanxi University of Science and Technology, Xi'an 710021, China

† Electronic supplementary information (ESI) available. See DOI: 10.1039/d0ra02029j

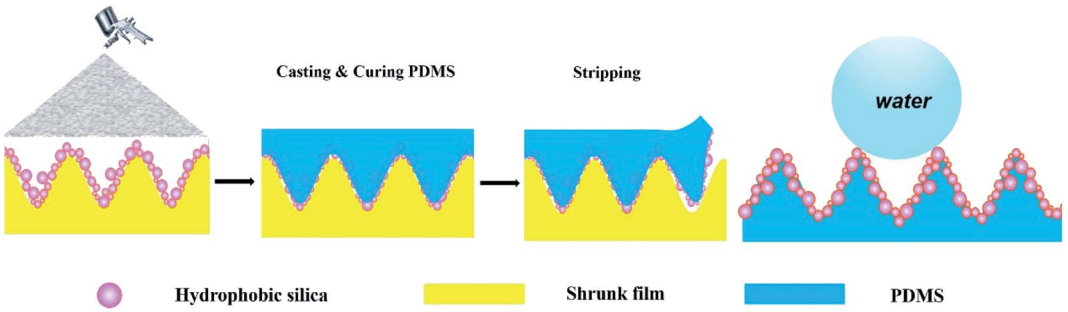

Fig. 1 A schematic illustration of the procedure used to prepare superhydrophobic PDMS/SiO_2 composite film.

nano roughness, and hydrophobization.[44] Although these results were encouraging, and the superhydrophobic characteristic could be maintained during deformation, these coatings are easily exfoliated from the substrate during relaxation because of weak adhesion between the substrate and the coating. Possible strategies to resolve these issues might include increasing cross-linking sites of coatings, and maintaining the substrate and roughening structures as a monolithic entirety.

The template method is a simple method to create roughened structures for superhydrophobic surfaces.[48,49] However, natural templates with rough structures from nature, such as lotus leaves, are not usually uniform due to the stems on the leaves, and do not easily allow the fabrication of materials with a large area. Furthermore, man-made master templates usually need special equipment to create roughened structures. In this study, we adopted a modified template to prepare a superhydrophobic composite film from a polymer-based shrink film which is easy to process using heat treatment. We prepared polydimethylsiloxane (PDMS)/SiO_2 composite films by spraying SiO_2 nanoparticles on a shrunken template with a micron hierarchical structure, and casting and curing the PDMS on the template, followed by stripping the composite film, as shown in Fig. 1. The film retained superhydrophobicity after tolerating ultraviolet (UV) irradiation for 150 h, sandpaper abrasion over 6 m with 100 g loading weight, weight pressing of 2000 g for 80 h, as well as immersion in acid (pH = 1), alkali (pH = 13) or organic solvents for 60 h. In addition, the as-prepared superhydrophobic composite films retained their anti-wettability under different strains, repeated stretching, and manual friction.

2 Experimental

2.1 Materials

Shrink film was purchased from Grafix. PDMS precursor and curing agent (Sylgard 184) were bought from Dow Corning (Australia). Silica nanoparticles (7–40 nm) were purchased from Aladdin. Octadecyltrimethoxysilane (purity: 90%) was provided from Macklin. Hexanol (purity ≥99.5%) and anhydrous ethanol (purity ≥99.0%) were obtained by Fuyu Fine Chemical Co. Ltd of Tianjin (China). All chemicals were used without further purification. Deionized water was bought from local supermarket.

2.2 Hydrophobic modification of silica nanoparticles

Hydrophobic silica nanoparticles were fabricated as follows: silica nanoparticles (1.5 g) were added into 80 mL of deionized water in 1000 mL beaker and stirred for 10 min at room temperature. Then ammonium hydroxide (40 mL) was slowly injected into the solution. Next, anhydrous ethanol (0.8 L) was added to the mixture. Subsequently, octadecyltrimethoxysilane (1.5 mL) was added to the system. The reaction was allowed to proceed for about 24 h under constant stirring at ambient temperature. After filtering, washing five times to neutral with anhydrous ethanol and drying at 60 °C for 24 h under vacuum, hydrophobic silica nanoparticles grafted with long-chain alkyl groups were obtained.

2.3 Fabrication of superhydrophobic film

Shrink film was cut into squares (7 cm × 7 cm), and washed with water. Once dry, the shrink film was put into oven at 175 °C for 5 min, then removed from the oven and allowed to cool to ambient temperature to obtain shrunk film.

Second, a dispersion of 1 wt% solution of hydrophobic silica nanoparticles in hexanol was sprayed onto the S-film using a spray gun (air pressure was maintained at 75 psi for spraying, the distance between the spray gun and the shrunk film was about 10 cm).

Subsequently, a measured amount of PDMS mixture semi-cured for about 15 min at 60 °C with precursors and curing agent (10 : 1 by weight) was poured onto the shrunk film with hydrophobic silica nanoparticles. After heating for 5 h at 60 °C, a cured PDMS/SiO_2 composite film with superhydrophobicity was obtained by stripping. The thickness of the composite film could be adjusted by controlling the amount of uncured PDMS poured on the shrunk film.

2.4 Characterization

Scanning electron microscopy (SEM) images were acquired on a Hitachi S-4800 field emission scanning electron microscope with an accelerating voltage of 5 kV. The sample was coated with gold prior to examination. CA measurements were performed with a video optical contact system (OCA 20, Dataphysics, Germany) at ambient temperature with 5 μL water droplet as the indicator, according to our work reported previously.[2,16,38] The CA value was read in about 10 s after the droplet was placed

steadily on the sample. The SA measurement was performed using tilting droplets. The lowest tilting angle that allowed a 10 μL water droplet to slide was recorded as the SA. The reported values of CA and SA were determined by averaging values measured at five different points on each sample surface.

2.5 Mechanical robustness testing

The mechanical durability of the PDMS/SiO_2 superhydrophobic composite film was tested by friction, pressing, and tensile forces. The friction tests were performed as follows: (1) the sample was cut into squares (30 mm × 30 mm) and placed down to the sandpaper with the rough side touching the sandpaper. The sample was moved 15 cm with a 100 g loaded weight across the sandpaper by an external force parallel to the substrate. The sample was rotated 90° clockwise and moved 15 cm further along the ruler to make sure the sample was abraded over several cycles; (2) a hand-friction test was performed by using gloved hands to rub the film. The pressing test was performed by pressing the composite film with 2000 g of weight. For the cyclic tensile test, the sample was fixed at both ends of the functional material testing machine (Goodtechwill, AI-7000-NGD). For cyclic stretching, the material was then subjected to cyclic stretching with a strain of 100%. The sample was stretched over 500 cycles.

2.6 Chemical stability

The chemical durability of the superhydrophobic composite film was evaluated by immersing the samples into aqueous solutions of different pH values and solvent for 60 h, before being rinsed with deionized water and dried.

2.7 UV irradiation resistance

The samples were subjected to UV irradiation using an artificial light source (UV lamp, Osram Ultra Vitalux 300 W) emitting a Gaussian-shaped spectrum peaking at 370 nm with a cut off at 290 nm. Samples were placed under the UV lamp for continuous irradiation at a distance of 20 cm between the UV lamp and the sample.

3 Results and discussion

3.1 Characterization of the PDMS/SiO_2 composite film

Surface microtopography has large influence on the wetting properties of a superhydrophobic surface. From Fig. 2a, it can be seen that the side-facing shrunk film became superhydrophobic with a micro-nano structure. The hierarchical surface displayed a typical Cassie state with a water CA up to 161° and an SA close to 0°. In this experiment, the dosage of nanoparticle dispersion sprayed on shrunk film is the most important factor relating to the obtained samples. The shrink film transformed from plain to highly wrinkled after heating (Fig. S1†). The corresponding superhydrophobic PDMS film is metastable, and the CA of the film reduced to less than 150° after 5 min (Fig. S2†). As shown in Fig. 2b, the hierarchical roughness consisted of a groove-bulge structure. On the microscale, a micro-texture was formed by the shrunk film with micron hierarchical structure. On the nanoscale, densely distributed nanoparticles appeared on each micro-groove and bulge (Fig. 2c and d). The high micro/nanoscale roughness created by well-designed micro-texture and the abundant nanoparticles provided sufficient room for "air pockets" between the patterned solid and water layer to form a Cassie–Baxter state.

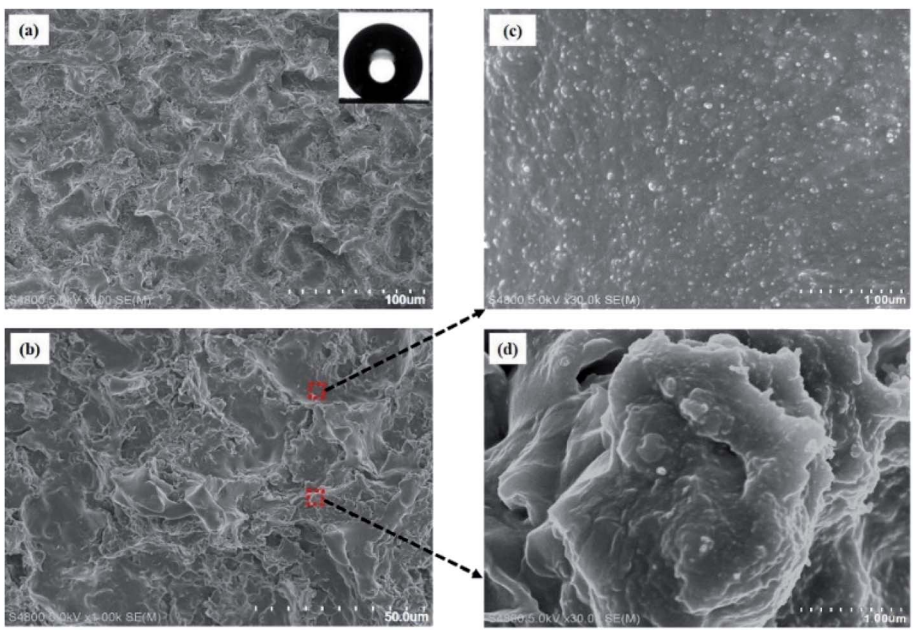

Fig. 2 (a and b) SEM images of superhydrophobic PDMS/SiO_2 composite film at different magnifications, showing nano-textured grooves (c) and bulges (d) at high magnification.

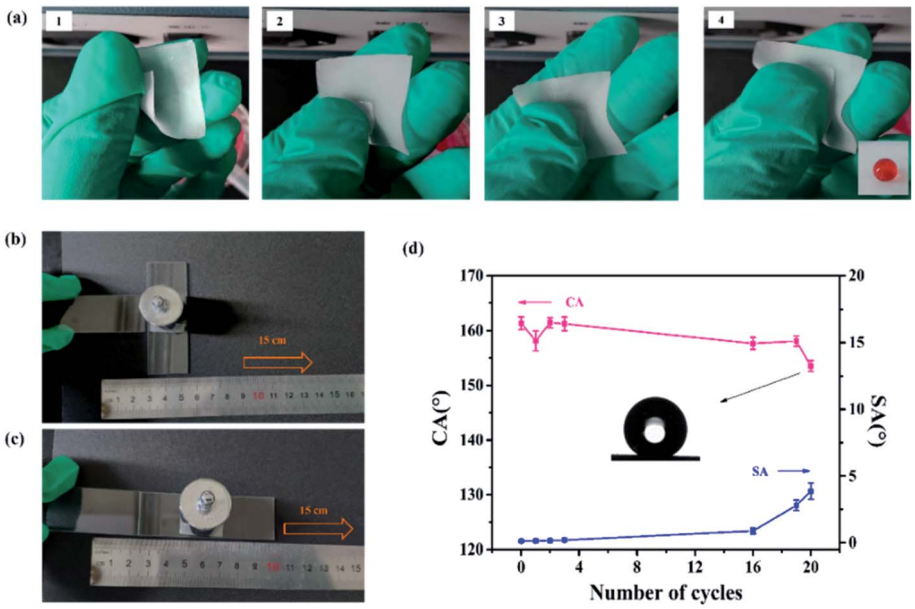

Fig. 3 (a) The process of producing man-made friction. (b and c) One cycle of sandpaper abrasion for superhydrophobic PDMS/SiO_2 composite film. (d) CAs and SAs of the superhydrophobic PDMS/SiO_2 film over 0–20 abrasion cycles on 240# sandpaper.

3.2 Mechanical stability

It is well known that the robustness and stability of superhydrophobic surfaces under the rubbing processes play a significant role in practical applications. To assess the robustness of our superhydrophobic surface, manual destruction and sandpaper abrasion were implemented to demonstrate the anti-wear properties of the superhydrophobic composite film. In the manual destruction, the surface was rubbed with two fingers back and forth (see the Video S1 in the ESI†). Fig. 3a shows screenshots of the Video S1.† After friction by hands, the superhydrophobic surface still retained water rolling properties. The water droplet flattened at the moment of contacting the film, then it bounced on the composite film without wetting or contaminating the surface (see the Video S2 in the ESI†), suggesting stable Cassie–Baxter state on the superhydrophobic surface. Here, resistance against mechanical damage was evaluated by abrading the sample using sandpaper to quantitatively evaluate the mechanical durability of the superhydrophobic surface.[50] The sandpaper test was carried out by loading a weight of 100 g onto the sample (Fig. 3b and c) and moving it across the sandpaper along a ruler. Fig. 3d demonstrates the changes in CA and SA as a function of the number of abrasion cycles. The superhydrophobic surface showed no obvious decay in CA and SA after the first three cycles. The CA decreased from 161.3 ± 1.2° to 153 ± 1.4°, and the SA of superhydrophobic surface was maintained at less than 5°, even after 20 abrasion cycles. As the number of abrasion cycles increased, the roughness of this superhydrophobic surface decreased, which may cause the loss of superhydrophobicity. Comparison of the results of the anti-abrasion test with those reported previously further confirm the excellent mechanical properties of the as-obtained superhydrophobic surfaces (Table S1†).

In addition to surface abrasion damage, the mechanical stability of the superhydrophobic film under stretching strain is extremely crucial. As shown in Fig. 4a, all CAs were still larger than 160° and SAs remained below 1° with increasing stretching strain to 100% from 0%. Fig. 4b show that a water droplet can maintain its spherical shape under different strains, indicating that the Cassie–Baxter state between the water and film was retained. Furthermore, the superhydrophobicity of the composite film could remain when it was returned to its initial position, and the film showed no deformation or damage with strain of 50% (see Video S3 in the ESI†). Fig. 4 shows the CAs and SAs of the superhydrophobic film under the stretching–relaxing procedure with a strain of 100%. It was found that the CAs of the film were still larger than 160°, whereas the SAs were still below 1° after the 500 cycles of stretching–releasing, indicating excellent adaptability to withstand mechanical cycles. The inset images of the water droplets before and after 500 cycles of the stretching–relaxing test demonstrate little difference. One cycle of tensile test is shown as Fig. 4d.

Generally, the loss of superhydrophobicity under large mechanical deformation is due to the transition of the Cassie–Baxter state to the Wenzel state. Thus, it is necessary to understand the state of our composite films under various strains. Here, we designed a simple model to analyze the wetting mechanisms. Fig. 5a depicts the structural deformation of hierarchical structure under stretching. We assume that the space distance between two micromastoids are grooves. When the superhydrophobic film was stretched, the grooves on the film became closely aligned parallel to the strain direction from random directions (Fig. 5b). Interestingly, the reorientation of the texture under stretching occurred only in the grooves (Fig. 5c). However, the structures on the microbulges were preserved under stretching (Fig. 5d). Microscale open air pockets remained between microbulges, and nanoscale sealed

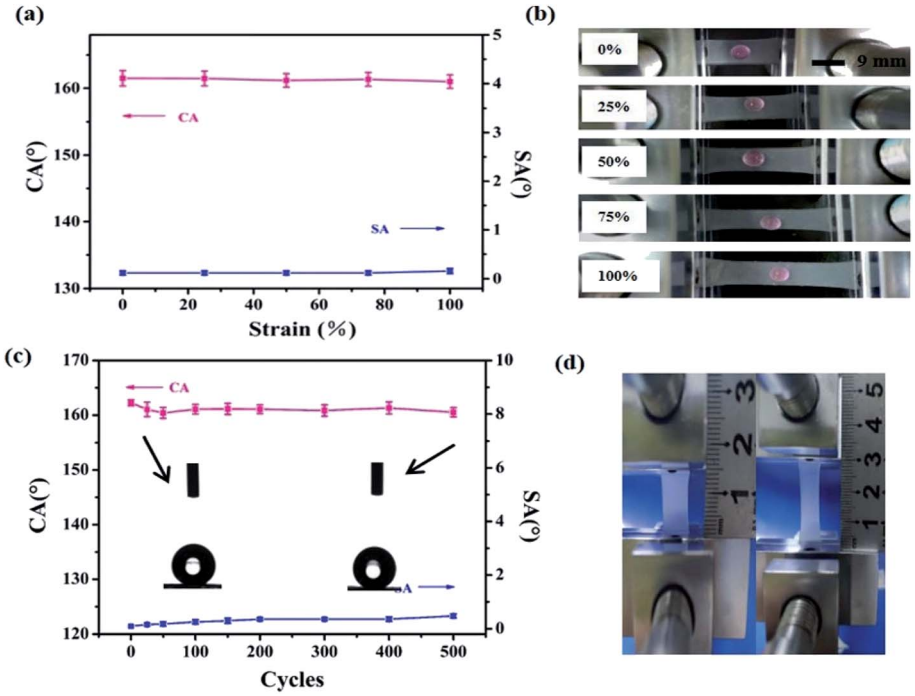

Fig. 4 (a) CAs and SAs of the superhydrophobic PDMS/SiO_2 film under different strains. (b) A water droplet can maintain its spherical shape under different strains. (c) CAs and SAs are over 155° and below 1° over numerous cycles with a strain of 100%. (d) Optical photographs of one cycle, the end cycle of tensile testing.

air pockets between nanomastoids on the microbulges. The open air pockets are connected to the atmosphere, contributing little to surface adhesive force and causing a high CA on the rough solid surfaces. All these changes still met the requirements of the Cassie state, and the composite film remained superhydrophobic.

In addition to the static parameters providing some information about the wetting properties, superhydrophobic surfaces show remarkable dynamic properties under the impact of droplets, which is important for the stability of Cassie–Baxter state. Herein, the behavior of a droplet impinging onto the surface of the relaxed film was recorded from side views (see the

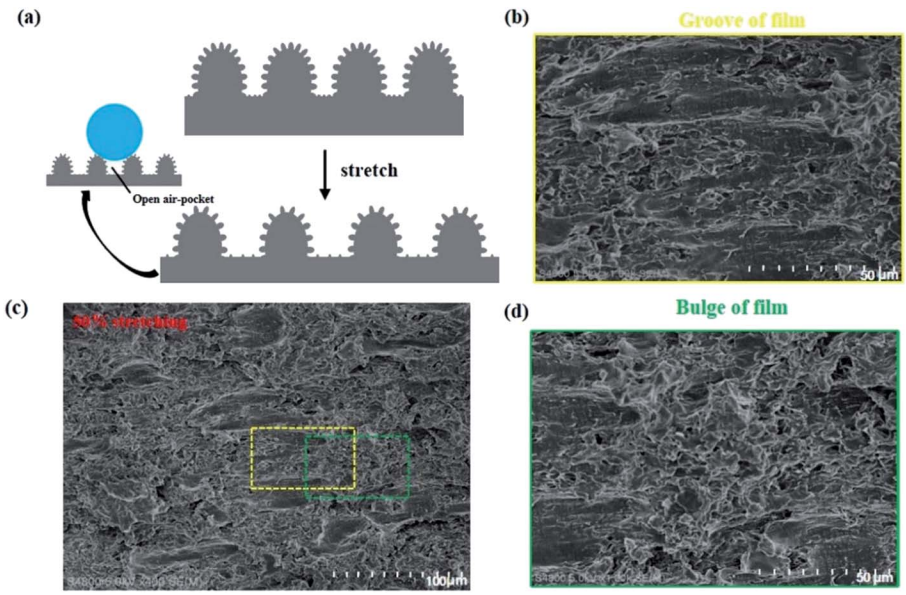

Fig. 5 A partial hydrophobic model of structure deformation under 50% tensile strain. (b–d) SEM images of stretched film (50% tensile strain); (b) and (d) showed zoomed in images of grooves and bulges from (c).

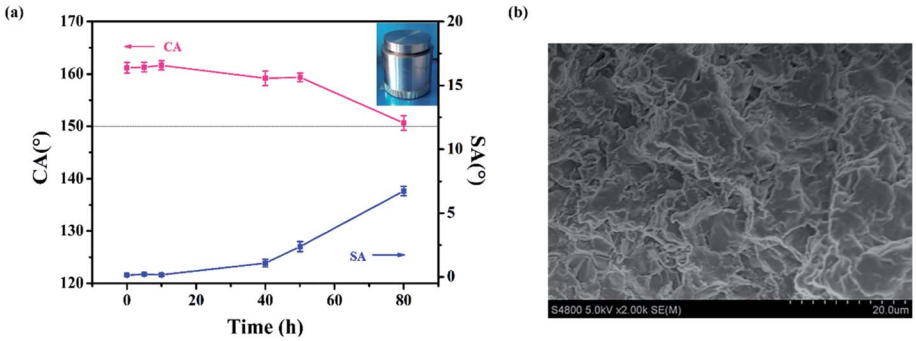

Fig. 6 (a) CAs and SAs of the film after pressing for different times under a 2000 g weight. (b) An SEM image of the superhydrophobic PDMS/SiO_2 film after pressing for 80 h under a 2000 g weight (the inset in (a) is a photograph of the pressing test model).

Video S4 in the ESI†). After contact with the surface, the droplet deformed first and flattened into the shape of a pancake, but then recoiled and finally rebounded off the surface without penetrating the nanostructure. The droplet rebounded completely, which suggests that a stable Cassie–Baxter state existed at the moment of impact. Superhydrophobic bouncing (see Video S5 in the ESI†) was maintained, even after mechanical stretching under 50% uniaxial strain. The almost complete rebound occurred on the stretched superhydrophobic surface when the dropping height of the water droplet increased (see Video S6 in the ESI†). We concluded that the behavior of water droplets dropping on stretched surfaces was nearly identical to that on hierarchical surfaces before stretching. The similar behavior of a droplet falling on the films was due to the stable Cassie–Baxter state of superhydrophobicity.

In practical applications, the pressure resistance of the film should be taken into consideration. Therefore, we evaluated the pressure resistance by placing a weight of 2000 g onto the sample, with the hierarchical side touching the weight.[51] The pressing test model is shown in the inset of Fig. 6a. From Fig. 6a, we can see that CA and SA only changed a little after the first 10 h of pressing. The CA of the PDMS/SiO_2 composite film decreased slightly, from 161.6 ± 1° to 159.2 ± 1.6°, and the SA increased to 1° after pressing for 40 h. When the pressing time reached 80 h, the CA decreased to about 150°, with SA still below 10°, showing the persistent superhydrophobicity of the composite film. The micromastoids on the surface became flat with increasing time, which lead to a reduction of roughness. Nevertheless, the nanostructures inside the grooves still remained (Fig. 6b). The composite film remained water-repellent, and the hierarchical structure of the composite film still retained the Cassie state.

3.3 Chemical durability and self-cleaning properties

We evaluated the chemical durability and robustness of the superhydrophobic film by dipping the samples in solution with

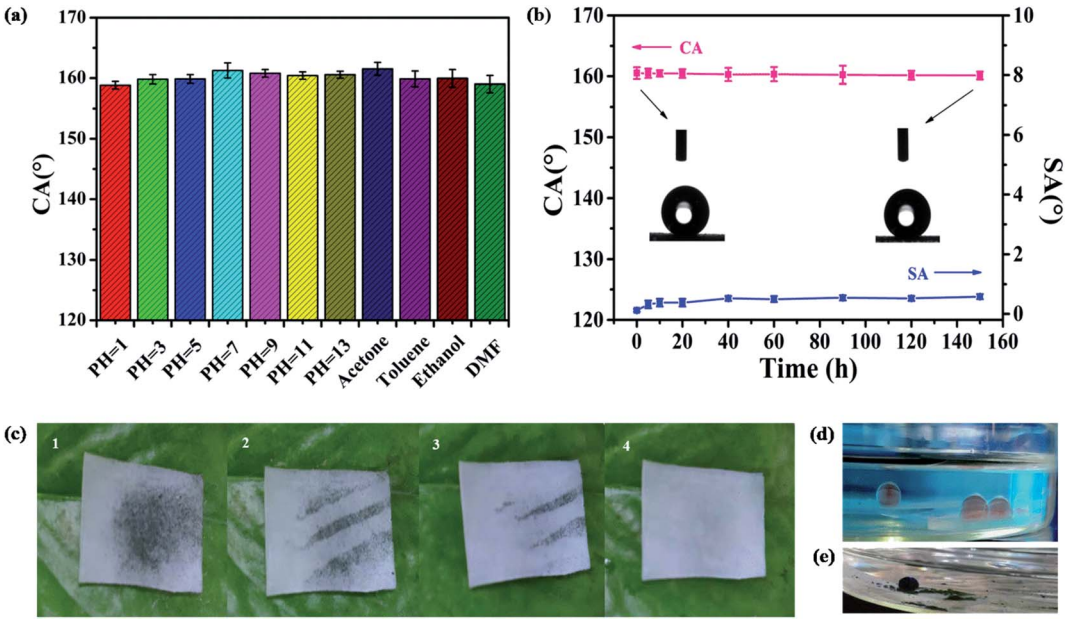

Fig. 7 (a) CAs of films treated by immersion in different pH solutions and various organic solvents for 60 h. (b) Changes in the CA and SA of film with UV irradiation time. (c) A self-cleaning test. (d) Water droplets sitting on the superhydrophobic PDMS/SiO_2 film under oil (left part) and on a glass slide (right part). (e) Methylene blue dissolved in water droplets, demonstrating spherical shapes under oil.

different pH values (pH = 1–13) and organic solvents for 60 h. Fig. 7a shows that the CA of the superhydrophobic film changed little, indicating strong resistance to different pH solutions. This phenomenon may be due to the air layer trapped on the surface, which can prevent acid or alkali from contacting samples. Additionally, after immersing in various organic solvents (toluene, acetone, ethanol, and dimethyl formamide [DMF]) for 60 h and washing with ethanol and water, then drying at 60 °C, the CAs of the samples remained above 155°, which indicated that all samples still retained superhydrophobicity. We compared the acidic/alkaline and solvent resistance of the PDMS/SiO_2 film with that of the reported superhydrophobic surfaces (Tables S2 and S3†). The as-obtained surfaces show longer stability than previous examples.

For the UV irradiation stability test, the sample was placed horizontally under the UV lamp at a distance of 20 cm. Fig. 7b shows that the CA and SA showed no obvious change after 150 h of irradiation, implying excellent resistance of the superhydrophobic film to UV light. The UV resistance was higher compared with samples reported in previous studies (Table S4†).

It is well known that the superhydrophobic surfaces have a self-cleaning property. When dirt falls on the surface, the rolling water droplets can remove the dirt. Here, methylene blue was applied as a marker of self-cleaning properties. From Fig. 7c, we can see that when the dye was washed with water droplets, the dry was easily removed by water droplet. In this work, the obtained superhydrophobic film also demonstrated self-cleaning properties in hexane. After being immersed in oil, the water droplets sat on the film demonstrating spherical shapes, and the water droplets spread and wet the hydrophilic glass surface (Fig. 7d). Methylene blue dissolved in the water droplet sitting on the superhydrophobic surface with a spherical shape, and the waste could easily be removed from the surface (Fig. 7e).

4 Conclusions

The template method usually requires complex technological processes and specialized equipment. Here, we have adopted a modified template to prepare stretchable and durable PDMS/SiO_2 superhydrophobic composite film. It was shown that the composite film, consisting of a PDMS elastomer, created superhydrophobic surfaces that were resistant to sandpaper abrasion, UV irradiation, chemical etching, and man-made friction. Importantly, the film with a groove-bulge structure has strong resistance to long term pressure. The modified template method might pave a new way to the fabrication of stretchable, anti-wetting materials.

Conflicts of interest

There are no conflicts to declare.

Acknowledgements

This work was supported by Natural Science Foundation of Shaanxi Province (2020JM-506), National Natural Science Foundation of China (51572161), and major project of Ministry of Science and Technology of China (2017YFB0307700).

Notes and references

1 Y. Wu, J. Zeng, Y. Si, M. Chen and L. Wu, *ACS Nano*, 2018, **12**, 10338–10346.
2 C.-H. Xue, Q.-Q. Fan, X.-J. Guo, Q.-F. An and S.-T. Jia, *Appl. Surf. Sci.*, 2019, **465**, 241–248.
3 H. Liu, J. Huang, Z. Chen, G. Chen, K.-Q. Zhang, S. S. Al-Deyab and Y. Lai, *Chem. Eng. J.*, 2017, **330**, 26–35.
4 X. Su, H. Li, X. Lai, Z. Chen and X. Zeng, *ACS Appl. Mater. Interfaces*, 2018, **10**, 10587–10597.
5 H. Gui, T. Zhang and Q. Guo, *ACS Appl. Mater. Interfaces*, 2019, **11**, 36063–36072.
6 M. Miwa, A. Nakajima, A. Fujishima, K. Hashimoto and T. Watanabe, *Langmuir*, 2000, **16**, 5754–5760.
7 Y. Tian, B. Su and L. Jiang, *Adv. Mater.*, 2014, **26**, 6872–6897.
8 X. Tian, T. Verho and R. H. A. Ras, *Science*, 2016, **352**, 142–143.
9 S. Wang, K. Liu, X. Yao and L. Jiang, *Chem. Rev.*, 2015, **115**, 8230–8293.
10 J. Li, L. Li, X. Du, W. Feng, A. Welle, O. Trapp, M. Grunze, M. Hirtz and P. A. Levkin, *Nano Lett.*, 2015, **15**, 675–681.
11 C.-H. Xue and J.-Z. Ma, *J. Mater. Chem. A*, 2013, **1**, 4146.
12 G. B. Hwang, A. Patir, K. Page, Y. Lu, E. Allan and I. P. Parkin, *Nanoscale*, 2017, **9**, 7588–7594.
13 S. Zhang, X. Ouyang, J. Li, S. Gao, S. Han, L. Liu and H. Wei, *Langmuir*, 2015, **31**, 587–593.
14 G. Zhang, S. Yuan, S. Cao, G. Yan, X. Wang, J. Yang and B. Van der bruggen, *Nanoscale*, 2019, **11**, 7166–7175.
15 D. Li, D. Wu and Z. Guo, *Nanoscale*, 2019, **10**, 6695–6703.
16 X.-J. Guo, C.-H. Xue, M.-M. Zhang, J.-Z. Ma and S.-T. Jia, *J. Mater. Chem. A*, 2015, **3**, 21797–21804.
17 Y. Cao, D. Zheng, X. Li, J. Lin, C. Wang, S. Dong and C. Lin, *ACS Appl. Mater. Interfaces*, 2018, **10**, 15150–15162.
18 S. S. Latthe, P. Sudhagar, A. Devadoss, A. M. Kumar, S. Liu, C. Terashima, K. Nakata and A. Fujishima, *J. Mater. Chem. A*, 2015, **3**, 14263–14271.
19 N. Wang, D. Xiong, Y. Deng, Y. Shi and K. Wang, *ACS Appl. Mater. Interfaces*, 2015, **7**, 6260–6272.
20 D. L. Hu, B. Chan and J. W. M. Bush, *Nature*, 2003, **424**, 663–666.
21 X. F. Gao and J. Lei, *Nature*, 2004, **432**, 36.
22 X. Gong, X. Gao and L. Jiang, *Adv. Mater.*, 2017, **29**, 1703002.
23 X. Su, H. Li, X. Lai, L. Zhang, X. Liao, J. Wang, Z. Chen, J. He and X. Zeng, *ACS Appl. Mater. Interfaces*, 2018, **10**, 4213–4221.
24 Z. Lian, J. Xu, Z. Wang, Z. Yu, Z. Weng and H. Yu, *Langmuir*, 2018, **34**, 2981–2988.
25 X. Su, H. Li, X. Lai, Z. Chen and X. Zeng, *Adv. Funct. Mater.*, 2019, **29**, 1900554.
26 W. K. Lee, W. B. Jung, D. Rhee, J. Hu, Y. L. Lee, C. Jacobson, H. T. Jung and T. W. Odom, *Adv. Mater.*, 2018, **30**, 1706657.
27 Y. Li, M. Ren, P. Lv, Y. Liu, H. Shao, C. Wang, C. Tang, Y. Zhou and M. Shuai, *J. Mater. Chem. A*, 2019, **7**, 7242–7255.
28 J. Peng, X. Zhao, W. Wang and X. Gong, *Langmuir*, 2019, **35**, 8404–8412.

29 I. Torun, N. Celik, M. Hancer, F. Es, C. Emir, R. Turan and M. S. Onses, *Macromolecules*, 2018, **51**, 10011–10020.
30 X. Zhang, W. Zhu, G. He, P. Zhang, Z. Zhang and I. P. Parkin, *J. Mater. Chem. A*, 2016, **4**, 14180–14186.
31 H. Wang, M. He, H. Liu and Y. Guan, *ACS Appl. Mater. Interfaces*, 2019, **11**, 25586–25594.
32 M. Zeng, P. Wang, J. Luo, B. Peng, B. Ding, L. Zhang, L. Wang, D. Huang, I. Echols, E. Abo Deeb, E. Bordovsky, C. H. Choi, C. Ybanez, P. Meras, E. Situ, M. S. Mannan and Z. Cheng, *ACS Appl. Mater. Interfaces*, 2018, **10**, 22793–22800.
33 X. Dong, S. Gao, J. Huang, S. Li, T. Zhu, Y. Cheng, Y. Zhao, Z. Chen and Y. Lai, *J. Mater. Chem. A*, 2019, **7**, 2122–2128.
34 L. Qin, N. Chen, X. Zhou and Q. Pan, *J. Mater. Chem. A*, 2018, **6**, 4424–4431.
35 H. Zhou, H. Wang, H. Niu, Y. Zhao, Z. Xu and T. Lin, *Adv. Funct. Mater.*, 2017, **27**, 1604261.
36 T. Lv, Z. Cheng, E. Zhang, H. Kang, Y. Liu and L. Jiang, *Small*, 2017, **13**, 1503402.
37 C. H. Xue, X. Bai and S. T. Jia, *Sci. Rep.*, 2016, **6**, 27262.
38 C. H. Xue, Z. D. Zhang, J. Zhang and S. T. Jia, *J. Mater. Chem. A*, 2014, **2**, 15001–15007.
39 S. Qiang, K. Chen, Y. Yin and C. Wang, *Mater. Des.*, 2017, **116**, 395–402.
40 M. Wu, B. Ma, T. Pan, S. Chen and J. Sun, *Adv. Funct. Mater.*, 2016, **26**, 569–576.
41 X. J. Guo, C. H. Xue, S. T. Jia and J. Z. Ma, *Chem. Eng. J.*, 2017, **320**, 330–341.
42 V. A. Ganesh, A. S. Nair, H. K. Raut, T. T. Yuan Tan, C. He, S. Ramakrishna and J. Xu, *J. Mater. Chem.*, 2012, **22**, 18479.
43 E. Huovinen, L. Takkunen, T. Korpela, M. Suvanto, T. T. Pakkanen and T. A. Pakkanen, *Langmuir*, 2014, **30**, 1435–1443.
44 S. J. Cho, H. Nam, H. Ryu and G. Lim, *Adv. Funct. Mater.*, 2013, **23**, 5577–5584.
45 J. Ju, X. Yao, X. Hou, Q. Liu, Y. S. Zhang and A. Khademhosseini, *J. Mater. Chem. A*, 2017, **5**, 16273–16280.
46 S. Wang, X. Yu and Y. Zhang, *J. Mater. Chem. A*, 2017, **5**, 23489–23496.
47 J. E. Mates, I. S. Bayer, J. M. Palumbo, P. J. Carroll and C. M. Megaridis, *Nat. Commun.*, 2015, **6**, 8874.
48 B. Bhushan, *Langmuir*, 2012, **28**, 1698–1714.
49 B. Bhushan, Y. C. Jung and K. Koch, *Philos. Trans. R. Soc., A*, 2009, **367**, 1631–1672.
50 M. Liu, J. Li, Y. Hou and Z. Guo, *ACS Nano*, 2017, **11**, 1113–1119.
51 W. K. Lee, W. B. Jung, S. R. Nagel and T. W. Odom, *Nano Lett.*, 2016, **16**, 3774–3779.